Dynamical Systems and Bio-medical Image Processing

DEMONGEOT J.
TIMC-IMAG
University J. Fourier of Grenoble
Faculty of Medicine 38 700 La Tronche
FRANCE

Abstract: - We present in this paper a series of operators coming from discrete (neural networks) or continuous (differential equations) dynamical systems and able to give adequate responses to low level image processing tasks like contrasting, segmenting and contouring objects of interest in bio-medical images. These operators are essentially based on a biomimetic approach, i.e. on the homogeneity reinforcement due to the lateral inhibition in retina or on the boundary enhancement due to chemotactic motion of bacteria. They realize image treatments in part analogous to those done by the natural vision and will be certainly improved by the new discoveries about natural and artificial retinas.

Key-Words: - Segmentation, Contrasting, Contouring, Bio-medical Images, Lateral Inhibition, Non-Isotropic Diffusion, Chemotactic Operator, Boundary Enhancement, Gaussian Stamping, Hamiltonian Contour.

1 Introduction

Like the medieval surgeon Henri de Mondeville whose Chirurgia in 1314 first proposed precise opening procedures based on the anatomy (Fig. 1), the modern surgical community [1] uses pre-treated anatomical images coming from the present imaging devices like MRI (Fig. 4). Pre-processing essentially involves after denoising 3 fundamental steps : contrasting, segmenting and contouring.

Figure 1: anatomic image from the Chirurgia by H. de Mondeville (1314)

The natural vision executes also these 3 tasks, the first being based on the architecture of the primary visual cortex which permits with the effect known as lateral inhibition the reinforcement of the image homogeneities. This effect is due to the fact that nearest neurons are exciting themselves and also inhibit the neurons of the next near layer ; it causes for example the Herman grid illusion, which empeaches the perception of all white circles in the Fig. 2, the black homogeneity forcing the peripheral circles to become grey, and in the same way it reinforces the homogeneous parts of an image (Fig. 3) in particular on its boundaries (Fig. 4) realizing concretely the Mach (boundary brightness overshoot) and the Marr (Laplacian 0-crossing edge enhancement) effects.

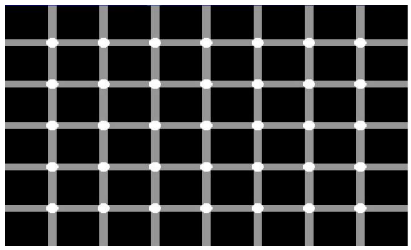

Figure 2: Herman illusion

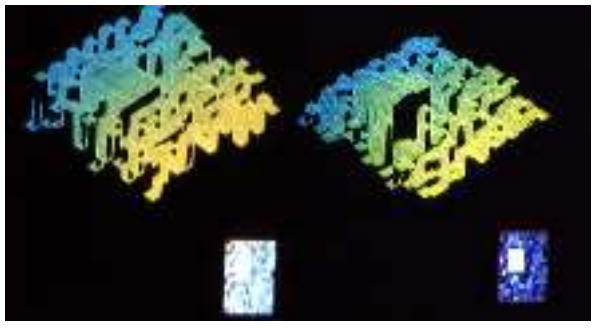

Figure 3: contrast enhancement with the initial image (left) and the contrasted image (right)

Because the objects of medical interest are often homogeneous with respect to their environment (a

tumour or an organ are made of cells coming from the same cellular clone), they are especially well enhanced by using lateral inhibition algorithms.

2 Discrete operators

If we call at time t G(t) the pixel grey level vector ($G(t)=\{g(i,t)\}_{i\in I}$, where g(i,t) is the grey level at the pixel i of the image I), J(t) the synaptic weights matrix, B(t) a threshold vector and h the Heaviside function, we can consider the following discrete neural networks operator:

$G(t+1)=h[J(t)G(t)-B(t)]$

$J(t)=J(t-1)+\gamma<G(t),G(t-1)>/\|G(t)\|$.

The second equation above is called the Hebbian rule and permits the progressive evolution of the image [2,3]. If J(0) respects the lateral inhibition rule, then it increases the correlations between the nearest neighbours components of G(t) having similar grey levels and contrarily pushes the very different components at distance 2 to vanish if they are very different from the components of a homogeneous region (cf. Fig. 4).

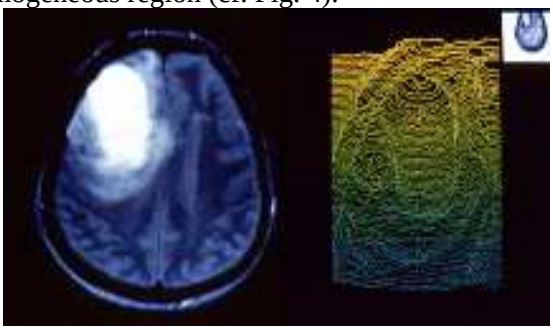

Figure 4: MRI image of tumour (left) and contrasted grey level at the border of the tumour (right)

The updating of the ò neuro-pixels Ó is in general parallel [4] allowing rapid calculations.

3 Continuous operators

3.1 A chemotactic operator

If we denote at time t g(x,t) the grey level function and b(x,t) the bacteria density at each image pixel x, we can consider the following equations, which constitute a new image processing operator [5]:

$\partial b/\partial t = L_b \left|\nabla g\right|_{max} \Delta b - \chi\nabla(b\nabla g)$,

$\partial g/\partial t = L_g \Delta g - Kg(b+\varepsilon)/(b+1)$,

with Neumann conditions on the image boundary.

These equations implies that the bacteria move towards the concentration of grey considered as a chemo-attractant to consume. They also diffuse as the grey level with respectively the viscosities L_b and L_g. The Fig. 5 below shows the progressive treatment of the image of a Chilean forest presenting the same characteristics of homogeneity than a tumour (the trees replacing the cells). After reaching its asymptotics, the dynamics of contrasting stops and can be followed by a contouring.

Figure 5: initial image of forest (top), asymptotic image (medium) and contouring (bottom)

3.2 A viability contouring operator

If we minimize the following functional [7], which provides a new snakes operator:

$[\alpha S(K(t)) + \beta V(K(t)) + \gamma\int_{\partial K(t)} 1/\|\nabla g(x)\|dx]$,

where K(t) is a compact object of interest moving toward a limit set K(°), we can obtain [6,7,8], by minimizing its external surface S as well as its inner volume V, real gloves (precise contour) contrarily to mittens (convex envelop) often observed with the Mumford-Kass-Terzopoulos algorithm (cf. Fig. 6).

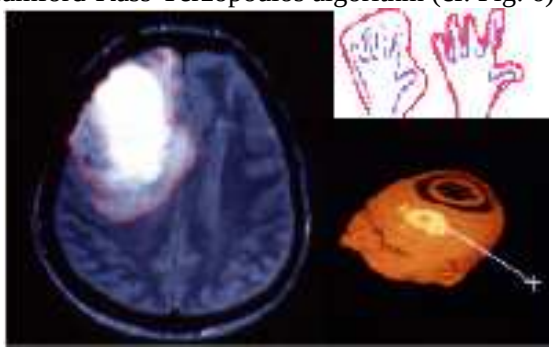

Figure 6: contouring the tumour of the Fig. 4 by using the viability operator above

We see on the Fig. 6 the use of the contouring done slice by slice before 3D spline smoothing for determining an optimal surgical trajectory (1). We

can impose to the contour to remain bicubic spline at each time step [7].

3.3 A scissor operator

The contouring after contrast enhancement can be also obtained by changing the location of the contour at each iteration passing locally from pixel p to pixel q (p→q), by minimizing the functional [9]:

$$\alpha|\Delta g(q)|+\beta/|\nabla g(q)|+\gamma|<\nabla g(p),pq>+\delta\int_{[p,q]}g(s)ds$$

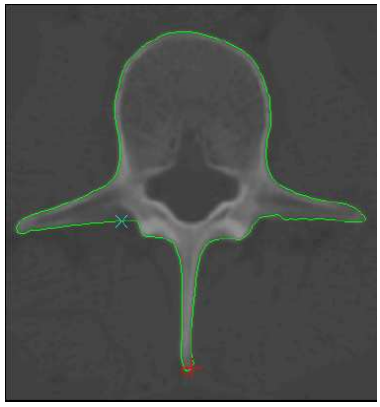

Figure 7: scissor asymptotic contour [8]

As in the viability contouring, which solves globally the problem of entering into the concavities of the boundaries, the scissor operator avoids the convex envelop of the objects of interest and well restitutes the aster like shapes (cf. Fig. 7)

3.4 A non-isotropic diffusion reaction operator

If we consider the grey level function g(x,0) as the initial image, we can follow the transient behavior of the well-known non-linear diffusion operator defined by [10]:

$\partial g/\partial t = Ldiv(\mathbf{1}_{[0,s]}(|\nabla(G_{*}g)|.\nabla g))$, with G~N(0,σ), and with Neumann conditions. The problem of this algorithm is that its asymptotics corresponds to a constant grey level suppressing the objects of interest inside the image (cf. Fig. 8).

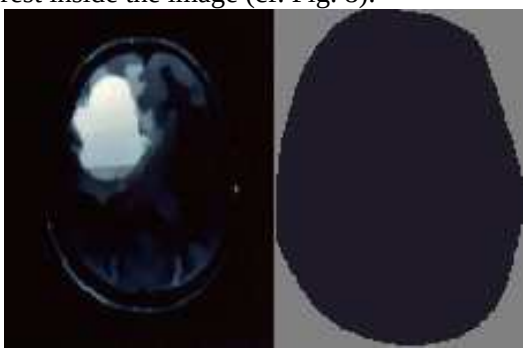

Figure 8: MRI image of the Fig. 4 treated at a transient step (left) and at its asymptotic state (right)

For that reason, we consider now a new non-isotropic reaction-diffusion operator defined in [5]:

$$\partial g/\partial t-div(L\nabla g)=0$$

$$dL/dt+L/\tau = P_{\nabla g}, \text{ if } |\nabla g|>s$$
$$=|\nabla g|^2 P_{\nabla g}+3(s^2-|\nabla g|^2)Id/2, \text{ if } |\nabla g|\dagger s,$$

where $P_{\mathbf{v}}.\|v\|$ is given by the matrix:

$$\begin{bmatrix} v_2^2 & -v_1v_2 \\ -v_1v_2 & v_1^2 \end{bmatrix}$$

In the equations above, the diffusion constant L becomes variable with the time t and its evolution equation is similar to the neural network operator described in Section 2. Treated images are obtained at the asymptotic state of the dynamics as for neural networks with lateral inhibition (cf. Fig. 9).

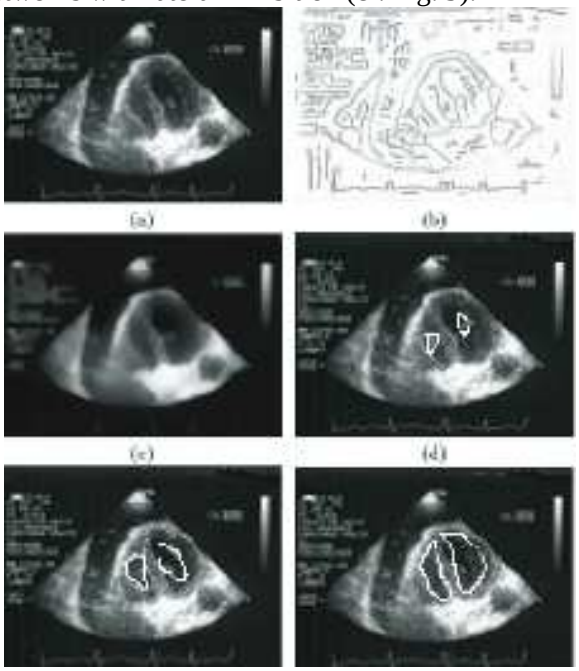

Figure 9: ultrasound image of the heart (top left), Canny-Deriche segmentation (top right), convergence to the asymptotics (medium left) and viability contouring (medium right and bottom)

3.5 Gaussian stamping

Let us define the characteristic line of a peak as the set of points where the mean Gaussian curvature of the peak vanishes (cf. Fig. 10 & 11). Its equation writes [11,12,13]:

$$H=\partial^2 g/\partial x^2\,\partial^2 g/\partial y^2 - (\partial^2 g/\partial x\partial y)^2 = 0$$

If H' = |H|, let consider the potential-Hamiltonian system obtained as follows:

$dx/dt = -\alpha\partial H'/\partial x[H(x,y)/G(x,y)] + \beta\partial H/\partial y$

$dy/dt = -\alpha\partial H'/\partial y[H(x,y)/G(x,y)] - \beta\partial H/\partial x,$

where $G(x,y)= \|\text{grad}(g)\|^2$.

Figure 10: grey landscape and characteristic lines

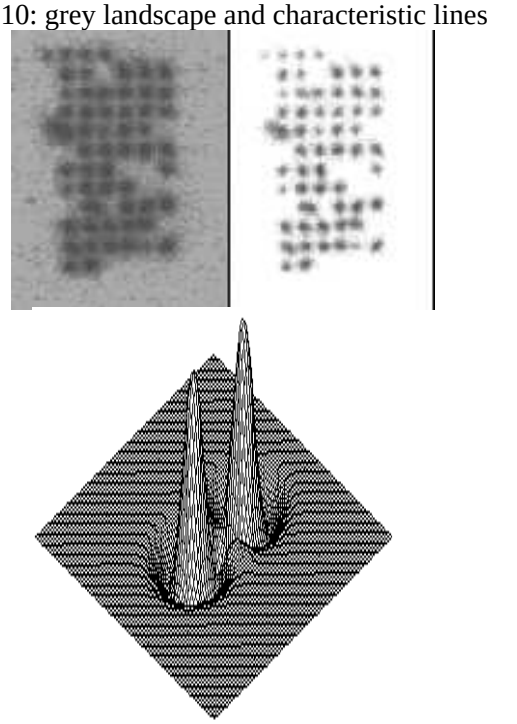

Figure 11: initial image of isotopic DNA chip (top left), filtered image (top right), function H for close peaks (medium), succeeding (separated peak, bottom left) and failed trajectories (close peaks, bottom right)

We have considered on Fig. 11 the new height function H(x,y) instead of the function g(x,y) at each pixel (x,y) and we have displayed after the plane potential-Hamiltonian differential system above of which the characteristic line is a limit cycle, called the Hamiltonian contour. Its first term is of steepest descent nature and along the flow, the orbits converge to the zeros of H'(x,y). On the set of the zeros of H'(x,y), the second Hamiltonian term of the differential system which is of convective type becomes preponderant. Parameters α and β can be used to tune the speed of convergence of the differential system to the limit cycle. The usual discretization of Runge-Kutta yields ultimately for the differential system an algorithm which is quite easy to implement. On each pixel (boundary effects are neglected), the function H(i,j) reads:

$$H(i,j)=[g(i+2,j)-2g(i+1,j)+g(i,j)][g(i,j+2)-2g(i,j+1)+g(i,j)]-[g(i+1,j+1)-g(i,j+1)-g(i+1,j)+g(i,j)]^2$$

An important property of the characteristic line is that in the case of a Gaussian peak, it contours the projection of a volume equal to 2/3 of the total volume of the peak. This property remains exact in case of moderate kurtosis and skewness of the peak. An advantage of this technique is that we do not perform a direct segmentation of the grey levels. Thus the segmentation is much finer than the corresponding one performed in the watershed lines method (or in its variant with markers). We only segment the upper part of the peak and we multiply by 3/2 the activity integrated in the interior of the characteristic line. This approach is interesting because the lower part of the peak is often noisy. The method seems particularly efficient when the peaks are well separated. If they are close (see Fig. 11), then we need to tune the parameters α and β.

Finally, we affect to each gene whose activity is represented by a peak on the DNA chip image (see Fig. 11) a standardized rectangle containing an activity coded through a grey level scale and eventually we reorganize (see Fig. 12) these rectangles in order to detect a co-expression of genes whose proteins are located in same part of the metabolic graph.

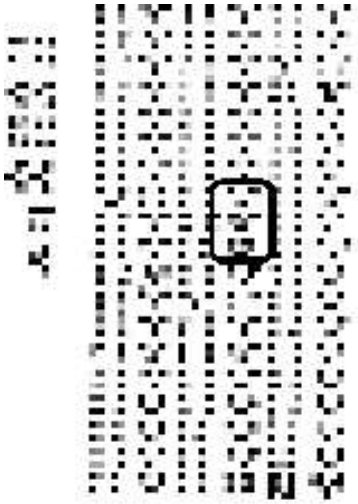

Figure 12: standardization of the DNA chip image (the black rectangle localize the sub-image treated in the Fig. 11 above)

3.6 Comparison with the watershed contouring

The watershed line is a concept firstly defined by geographers in order to characterize the main features of a landscape [14-18]: a drop of rain that reaches the ground will flow down to a sea or an ocean. In the case of France, the watershed line splits the country in two parts, the atlantic zone and the mediterranean zone. Those zones are called 'catchment basins', and the oceans are the minima of them. They define a partition of the relief, and the frontiers of catchment basins define on the pixels plane the watershed line. We can easily understand the interest of this concept in image processing: grey level images can be considered as relief structures, and the watershed line is a good way to separate light (low) zones from dark (high) ones. It is particularly interesting to determine the watershed line of the symmetrical landscape obtained by considering the new grey level 1-g, where g is the initial normalized grey level (if we have taken the maximum of g as a normalized value equal to 1). The watershed line verifies a variational principle: when progressively fulfilling with water a catchment basin, its inner area passes through a series of inflexion points corresponding to the successive saddle points reached by the water. Each inflexion point corresponds to a local maximum of the second derivative of this inner area.

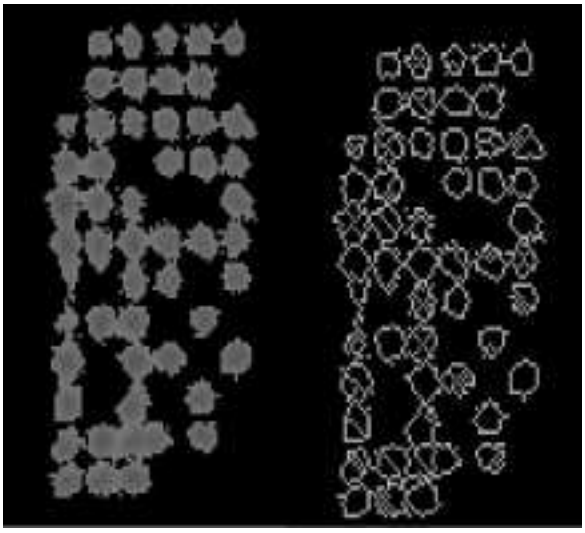

Figure 13: the DNA chip image of the Fig. 11 treated by a watershed method (left) and the corresponding contouring (right)

The watershed line is computed on discrete image, by immersion simulation, locating the watershed line on the meeting points of several catchment basins (cf. Fig. 13). First discrete algorithms of watershed computing by immersion simulation were proposed in [19-22] for a discrete operator related to the watershed. In our case, the watershed line is computed on the inverse image, in order to have one and only one local maximum (of the original image) into each catchment basin. Then the resulting labelling (still not a partition) is used on the original image. We used the Vincent-Soille algorithm [14] on discrete images with a linear complexity (about 7,25 N, where N denotes the number of pixels in the image), which can be used also in 3 dimensions.

4 Conclusion and outlook

We have proposed in this paper a collection of methods for solving tasks of low level image processing like contrasting, segmenting and contouring. A common feature of all these methods is the use of dynamical systems (both discrete and continuous) transforming the initial grey landscape in an asymptotic image representing the final state of the processing. The dynamical methods used for treating medical images will certainly know a rapid development parallel to those of the diffusion-reaction operators often used to model biological systems. These operators are indeed very robust to parameter changes and well studied mathematically, especially concerning the existence and unicity of solutions and also for all problems related to the convergence to their asymptotic state. They realize image treatments in part analogous to those done by the natural vision [23] and will be certainly improved by the new discoveries about natural and artificial retinas. The general present tendency to copy the natural vision processing and cognitive treatment in the human brain for finding new pertinent image processing algorithms will also push in the same direction. We could call this general movement the dynamical bio-image processing: it proposes a unified methodology for processing bio-images and for explaining the dynamical phenomenology observed inside these bio-images. Because these methods often suggest adapted acquisition devices acquiring only the variables necessary to feed the future modelling of the dynamical objects of interest inside the bio-images or to allow their matching [24], we can finally consider the possibility of a feedback on the primary level of acquisition we could call the dynamical model driven acquisition. The whole methodology made of the dynamical bio-image processing and of the dynamical model driven acquisition could be defined as the dynamical bio-imaging and could be useful in the medical and biological community for studying the complex dynamical living systems.

Acknowledgements:
We are deeply indebted to the Institut Universitaire de France for giving during 10 years the

opportunity to perform the research presented in this paper. This long support has been obtained by the unvaluable efforts by C. All gre. I thank also my students F. Berthommier, G. Ionescu, J. Mattes and M. Richard for our numerous fruitful discussions.

References:

[1] A.L. Benabid, P. Cinquin, S. Lavall e, J.F. Le Bas, J. Demongeot & J. de Rougemont, A computer driven robot for stereotactic surgery connected to cat-scan magnetic resonance imaging, *Applied Neurophysiology*, 50, 1987, pp. 153-154.

[2] L. Brunie, F. Leitner, F. Berthommier, P. Cinquin & J. Demongeot, Interpretation of multimodal medical images using connectionist and variational methods, *Technology and Health Care*, 3, 1995, pp. 91-100.

[3] L. Brunie, F. Leitner, F. Berthommier, P. Cinquin & J. Demongeot, Interpretation of multimodal medical images using connectionist and variational methods, *Technology and Health Care*, 3, 1995, pp. 91-100.

[4] J. Mattes, D. Trystram & J. Demongeot, Parallel image processing using neural networks: applications in contrast enhancement of medical images, *Parallel Processing Letters*, 8, 1998, pp. 63-76.

[5] J. Demongeot, S. Meignen, F. Leitner, M. El Ayyadi & G.H. Cottet, New tools in medical imaging, *J. Theor. Med.*, in revision.

[6] F. Leitner, P. Paillasson, X. Ronot & J. Demongeot, Dynamical, functional and structural analysis of living cells : new tools for vital staining of nuclear DNA, *A c t a Biotheoretica*, 43, 1995, pp. 299-317.

[7] J. Demongeot & F. Leitner, Compact set valued flows I : applications in medical imaging, *C.R. Acad. Sc.* S rie IIb, 323, 1996, pp. 747-754.

[8] T. Lorenz, Compact set valued operator, *Comp. Vis. Sci.*, 4, 2001, pp. 41-57.

[9] E.N. Mortensen & W.A. Barrett, Interactive segmentation with intelligent scissors, *Graph. Models & Image Proc.*, 60, 1998, pp. 349-384.

[10] L. Alvarez, P.L. Lions & J.M. Morel, Image selective smoothing and edge detection by nonlinear diffusion, *SIAM Journal on Numerical Analysis*, 29, 1992, pp. 845-866.

[11] J. Demongeot, J.P. Fran oise, M. Richard, F. Senegas & T.P. Baum, A differential geometry approach for biomedical image processing, *C. R. A. S. Biologies*, 325, 2002, pp. 367-374.

[12] J. Demongeot, J. Bezy-Wendling, J. Mattes, P. Haigron, N. Glade & J.L. Coatrieux, Multiscale Modeling and Imaging: The Challenges of Biocomplexity, *Proc. IEEE* , 91, 2003, pp. 1723-1737.

[13] J. Aracena, S. Ben Lamine, M.A. Mermet, O. Cohen & J. Demongeot, Mathematical modelling in genetic networks˚: relationships between the genetic expression and both chromosomic breakage and positive circuits, *IEEE Trans. Systems Man Cyber.*, 33, 2003, pp. 825-834.

[14] L. Vincent & P. Soille, Watershed in Digital Spaces: an Efficient Algorithm Based on Immersion Simulations, *IEEE Transactions on Pattern analysis and Machine Intelligence*, 13, 1991, pp. 583-598.

[15] F. Meyer, Un algorithme optimal de ligne de partage des eaux, in: VIII me Conf. Reconnaissance des Formes et Intelligence Artificielle, *AFCET*, Paris, 1992,˚pp. 847-859.

[16] S. Beucher & F. Meyer, The morphological approach to segmentation: the watershed transformation, in: Dougherty E.R., (Ed.), Mathematical Morphology in Image Processing, *Marcel Dekker*, New York, 1993, pp. 433-481.

[17] G. Bertrand, J.C. Everat & M. Couprie, Topological gray scale watershed transformation, Vision Geometry VI, *SPIE*, 3168, 1997, pp. 136-146.

[18] G. Bertrand, J.C. Everat & M. Couprie, Image segmentation through operators based upon topology, *Journal of Electronic Imaging*, 6, 1997, pp. 395-405.

[19] J. Mattes, M. Richard & J. Demongeot, Tree representation for image matching and object recognition, *Lecture Notes in Comp. Sc.*, 1568, 1999, pp. 298-309.

[20] J. Mattes & J. Demongeot, Dynamic confinement, classification and imaging, *Studies in Classification and Data Anal.*, 14, 1999, pp. 205-214.

[21] J. Mattes & J. Demongeot, Tree representation and implicit tree matching for a coarse to fine image matching algorithm, *Lecture Notes in Comp. Sc.*, 1679, 1999, pp. 646-655.

[22] G. Ionescu, S. Lavall e & J. Demongeot, Automated registration, *Lecture Notes in Comp. Sc.*, 1679, 1999, pp. 768-777.

[23] N. Ohyama, C.M. Yamaguchi & C.H. Haneishi, Concept & Technologies of human vision, *Proceedings IDW02*, 2002, pp. 11-14.

[24] G. Palos, N. Betrouni, V. Devlaminck & J. Rousseau, Fast nonrigid matching of multimodality medical images, *WSEAS Trans. Biol. Biomed.*, 1, 2004, pp. 99-102.